ADVANCED ENERGY MATERIALS
www.advenergymat.de

Materials Views
www.MaterialsViews.com

Dual-Function Air Cathode for Metal–Air Batteries with Pulse-Power Capability

Jeffrey W. Long, Christopher N. Chervin, Nathan W. Kucko, Eric S. Nelson, and Debra R. Rolison**

We demonstrate that air-breathing electrodes comprising carbon nanofoam papers painted with conformal nanoscale coatings of manganese oxide (MnO*x*) exhibit both energy storage and conversion function by providing electrocatalytic activity for oxygen reduction plus faradaic pseudocapacitance associated with Mn(III/IV) redox in the oxide. This property combination, difficult to achieve in a single electrode material, allows the oxide-derived pseudocapacitance to sustain seconds-long discharge pulses at rates that cannot be met by oxygen reduction alone. Manganese (III) sites in the post-pulsed oxide spontaneously recharge to Mn(IV) in the presence of oxygen—making the oxide ready and available for subsequent pulse-power discharge.

Electrochemical energy-storage devices typically occupy a narrow performance space within the power *vs.* energy spectrum as represented by the Ragone plot.[1] Batteries are a common choice when high specific energy is desired, but may not be up to the task for applications that require high power (energy-per-unit-time).[2] Electrochemical capacitors (ECs) deliver pulse power on the timescale of seconds or less, but at an order of magnitude lower specific energy than that provided by batteries.[3–5] The complementary characteristics of batteries and ECs can be married in a hybrid device that contains both discrete components, but complex control electronics are often required to manage the energy/power profiles of such hybrid devices.[6,7] Alternatively, both functions—specific power and specific energy—can be imparted to a single device by redesigning the energy-storing interphase using an architectural and nanoscopic perspective.[8,9]

Metal–air batteries use molecular oxygen from air as the primary reactant at the positive electrode, thereby yielding the highest specific energy among common battery chemistries, with the commercial exemplar being the primary Zn–air battery.[2,10] While providing exceptional specific energy (up to 400 W h kg^{-1}) with the added safety benefits and affordability of aqueous cell chemistry, Zn–air batteries lack the pulse-power capability required by many emerging applications.[11] The physical structure of the air cathode must support multiple tasks—O_2 transport, ion transport, electron conduction, electrocatalytic reactivity—and is currently fabricated via "brick-and-mortar" methods to form a powder-composite electrode of carbon black, catalyst particles (typically manganese oxides),[12,13] and polymeric binder. Although functional as an air cathode, the ad hoc distribution of transport pathways in the typical composite electrode structure restricts its ability to provide on-demand pulse power.

We now report that the redesign of air cathodes using a "multifunctional electrode nanoarchitecture"[14] approach unleashes dual functionality at the nanoscale MnO*x* coating—oxygen reduction to sustain long-term energy delivery and faradaic electron/cation charge-storage reactions to provide intermittent, short-term discharge pulses (tens of seconds), as schematically shown in **Figure 1**. The base architecture for this electrode design begins with fiber-paper-supported carbon nanofoams, which are "plug-and-play" electrode platforms that can be scaled in *x* and *y* (to 10s of cm^2) and *z* (60–540 μm).[15] Ultrathin (~10 nm), conformal coatings of Na^+-birnessite-type MnO*x* are applied to the interior and exterior surfaces of the nanofoam papers via reaction with aqueous permanganate solutions.[16–18] Because the deposition is performed under self-limiting conditions, the pore structure of the native nanofoam is retained after MnO*x* deposition, as verified by scanning electron microscopy (Figure 1); X-ray energy dispersive spectroscopy confirms the presence of MnO*x* homogeneously dispersed on the carbon surface (Supporting Information, SI). The MnO*x* weight loading can be varied based on exposure time in the permanganate solution;[17] for the present studies we examined carbon nanofoam papers with 20 and 40 wt.% MnO*x*.

The MnO*x*–carbon nanoarchitectures were originally developed to deliver pseudocapacitance-based pulse power in electrochemical capacitors.[16–20] More recently, we demonstrated that related MnO*x*–carbon structures serve as effective air-breathing cathodes with alkaline electrolytes, once the hydrophilic MnO*x*-modified nanofoam is coated with a boundary layer of hydrophobic polymer (poly(vinylidenedifluoride), PVdF) to limit electrolyte flooding into the interior.[21] On the basis of these findings, we down-selected a particular nanofoam formulation with pores on the order of 100–200 nm and 270-μm thickness, a structure that exhibits the highest oxygen-reduction activity among the nanofoam-based air cathodes we have investigated to date. For electrochemical evaluation we designed an air-breathing electroanalytical cell based on a modified three-electrode cell (see SI) in which one face of the nanofoam cathode is exposed to gas (flowing argon or static air) while the opposing face contacts a gel electrolyte

J. W. Long, C. N. Chervin, N. W. Kucko,
E. S. Nelson, D. R. Rolison
Code 6170, Surface Chemistry Branch
U. S. Naval Research Laboratory
4555 Overlook Avenue SW, Washington, DC, 20375, USA
E-mail: jeffrey.long@nrl.navy.mil; rolison@nrl.navy.mi

DOI: 10.1002/aenm.201200921

Report Documentation Page

Form Approved
OMB No. 0704-0188

1. REPORT DATE	2. REPORT TYPE	3. DATES COVERED
2013		**00-00-2013 to 00-00-2013**

4. TITLE AND SUBTITLE	5a. CONTRACT NUMBER
Dual-Function Air Cathode for Metal-Air Batteries with Pulse-Power Capability	5b. GRANT NUMBER
	5c. PROGRAM ELEMENT NUMBER
6. AUTHOR(S)	5d. PROJECT NUMBER
	5e. TASK NUMBER
	5f. WORK UNIT NUMBER
7. PERFORMING ORGANIZATION NAME(S) AND ADDRESS(ES) **U. S. Naval Research Laboratory,4555 Overlook Avenue SW,Washington,DC,20375**	8. PERFORMING ORGANIZATION REPORT NUMBER
9. SPONSORING/MONITORING AGENCY NAME(S) AND ADDRESS(ES)	10. SPONSOR/MONITOR'S ACRONYM(S)
	11. SPONSOR/MONITOR'S REPORT NUMBER(S)

12. DISTRIBUTION/AVAILABILITY STATEMENT
Approved for public release; distribution unlimited

13. SUPPLEMENTARY NOTES
Adv. Energy Mater. 2013, 3, 584-588

14. ABSTRACT

15. SUBJECT TERMS

16. SECURITY CLASSIFICATION OF:			17. LIMITATION OF ABSTRACT	18. NUMBER OF PAGES	19a. NAME OF RESPONSIBLE PERSON
a. REPORT **unclassified**	b. ABSTRACT **unclassified**	c. THIS PAGE **unclassified**	**Same as Report (SAR)**	**6**	

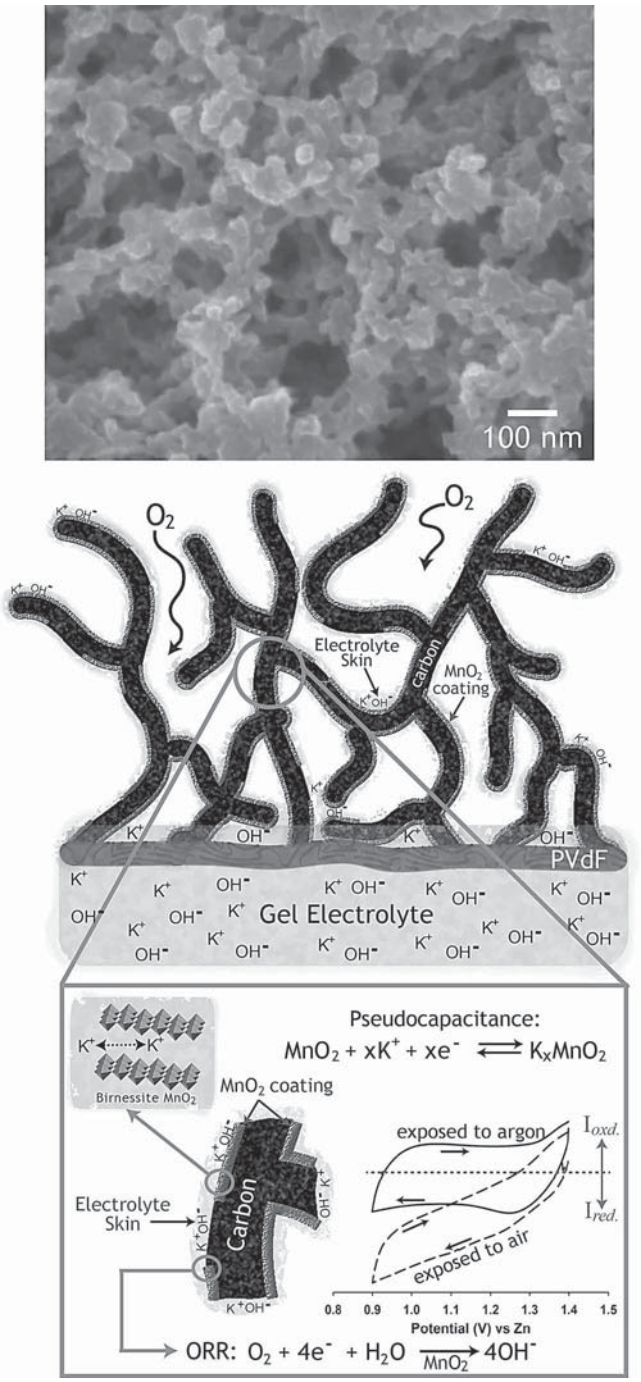

Figure 1. (Top) scanning electron micrograph of MnO*x*-coated carbon nanofoam paper; (middle) schematic of nanofoam-based air cathode with internal surfaces wetted by alkaline electrolyte and infused with O_2(*g*); (bottom) schematic of multiple electrochemical processes that occur during dual-function air cathode operation.

(poly(acrylic acid), PAA, and 6 M KOH) that also contains a Zn wire quasi-reference electrode (QRE) and a large Pt gauze counter electrode.

The baseline O_2-reduction activity for both native and MnO*x*-modified nanofoams is established by potential-step experiments on air-exposed nanofoam electrodes (**Figure 2**a). Manganese oxides are well-established catalysts for O_2 reduction in alkaline media, where MnO*x* promotes disproportionation of the peroxide that forms upon two-electron reduction of O_2, ideally resulting in an overall four-electron process.[22–24] The addition of conformal coatings of nanoscale MnO*x* birnessite to the carbon nanofoam enhances O_2-reduction activity in two ways to achieve values technologically relevant for air-cathodes: shifting the onset potential positive (by ~100 mV) and increasing total current density (4–6× greater at high overpotential), Figure 2a.[21] Oxygen-reduction activity does not necessarily track MnO*x* weight loading, but typically reaches a maximum between 20 and 40 wt.% MnO*x* for oxide-modified carbon nanofoam papers. At MnO*x* loadings higher than 40 wt.%, O_2-reduction activity decreases, possibly due to more extensive electrode flooding and/or obstruction of pores by thicker MnO*x* coatings.

The presence of nanoscale MnO*x* also amplifies the capacitance relative to the native carbon nanofoam, as observed by cyclic voltammetry of argon-bathed nanofoam electrodes (Figure 2b). Higher current density and corresponding capacitance are exhibited by the MnO*x*–carbon nanofoam papers because of Mn(III/IV) faradaic reactions (Figure 1) whose potential–current profile mimics double-layer capacitance.[16,19,25–27] The capacitance enhancement roughly tracks the weight loading of MnO*x* in the electrode architecture. Geometric area-normalized capacitances derived from cyclic voltammetry at 5 mV s^{-1} are 0.8, 2.4, and 3.3 F cm^{-2} for the native, 20 wt.%, and 40 wt.% MnO*x*-modified carbon nanofoam papers, respectively. Corresponding specific capacitances, normalized to the total mass of the electrodes, are 25, 40, and 58 F g^{-1}, respectively.

We previously examined related MnO*x*–carbon nanofoams in a conventional three-electrode cell under conditions where the nanofoam electrode was intentionally flooded with alkaline electrolyte (1.5 M LiOH + 5.6 M KOH) via vacuum infiltration. Under such conditions MnO*x*–carbon nanofoams with comparable MnO*x* loadings exhibit 150 F g^{-1} total electrode.[19] With PVdF-coated MnO*x*–carbon nanofoam papers that were adventitiously wetted with alkaline gel electrolyte in the air-breathing cell configuration, specific capacitance is three-fold lower, indicating that only a fraction of the MnO*x* is electrochemically accessible at the timescales examined. Underutilization of the MnO*x* pseudocapacitance may arise from incomplete wetting of the internal surfaces of the MnO*x*-coated carbon nanofoam and/or electrolyte starvation caused by local depletion of charge-compensating ions that support Mn(III/IV) redox cycling.[20] For the next stage in the evolution of carbon nanofoam-based air cathodes, we will develop methods to incorporate more deliberate ion-conducting pathways throughout the electrode volume, while still maintaining open porosity for O_2 transport.

Galvanostatic measurements permit us to query the nanofoams under conditions that are more typical of a functioning battery and allow pulsed interrogation of the air cathode in the electroanalytical cell. Under constant-current load and in an argon atmosphere, MnO*x*-modified nanofoam papers provide more capacity than the native nanofoam paper as seen by extension of the discharge time to reach a selected potential

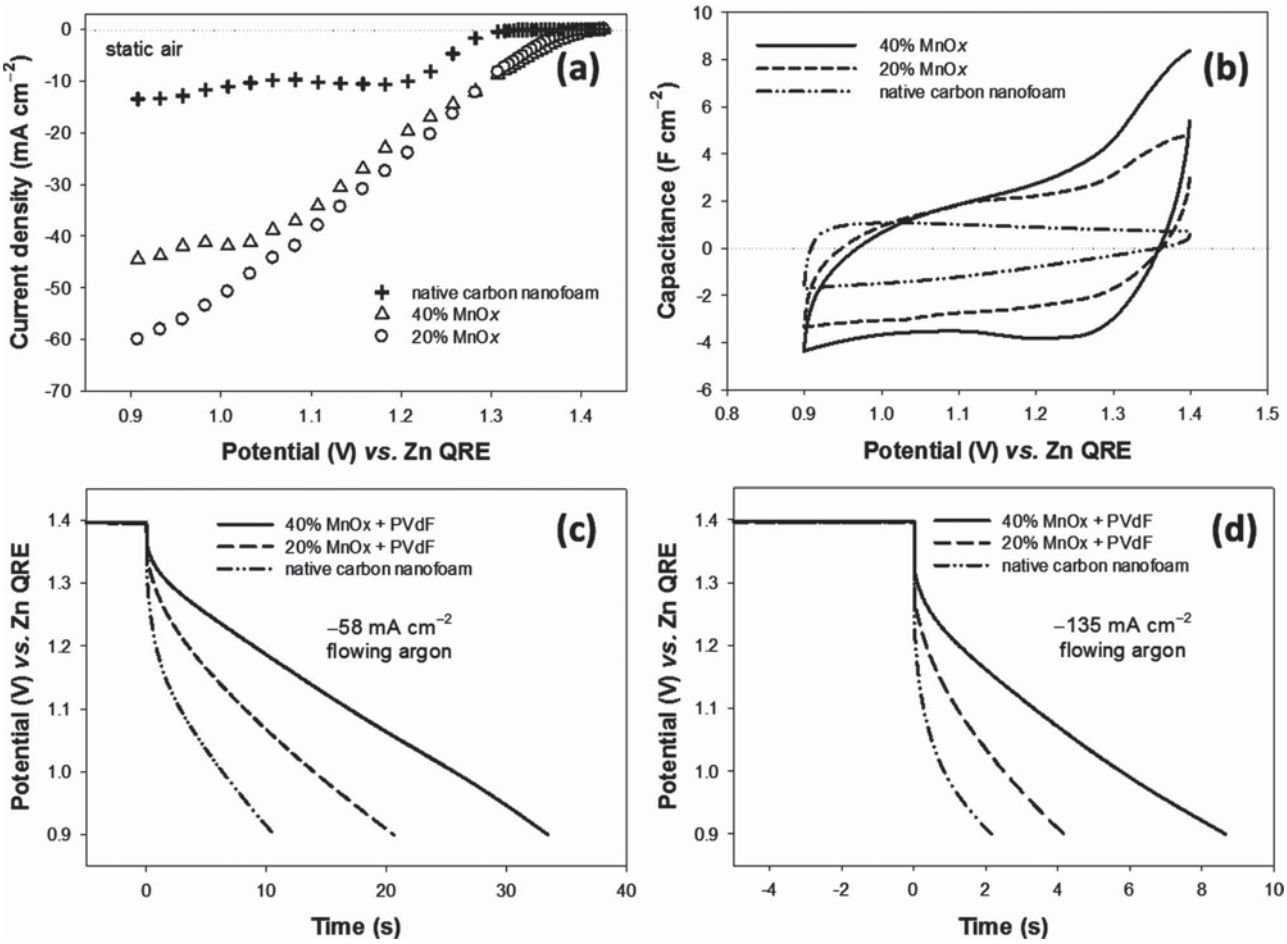

Figure 2. (a) Steady-state current–potential response in 6 M KOH/PAA electrolyte of (Δ) 40 wt.% MnO*x*-modified nanofoam paper, (O) 20 wt.% MnO*x*-modified nanofoam paper, and (+) native carbon nanofoam paper; the steady-state currents were recorded 20 min after each potential step (from 1.425 to 0.9 V vs. Zn QRE); (b) cyclic voltammograms in 6 M KOH/PAA at 5 mV s^{-1} for (—) 40 wt.% MnO*x*-modified nanofoam paper; (– –) 20 wt.% MnO*x*-modified nanofoam paper, and (–••–) native carbon nanofoam paper. Galvanostatic discharge profiles in 6 M KOH/PAA under flowing argon are shown for current densities of (c) –58 mA cm^{-2} and (d) –135 mA cm^{-2} for (—) 40 wt.% MnO*x*-modified nanofoam paper, (—) 20 wt.% MnO*x*-modified nanofoam paper, and (–••–) native carbon nanofoam paper. The electrode geometric area is defined as the area of the circular hole cut in the nickel-foil current collector.

limit (see Figure 2c). For the 40 wt.% MnO*x*–carbon nanofoam, the area-normalized capacitance values as determined from galvanostatic measurements are 4.5, 3.9, and 3.6 F cm^{-2} at current densities of –58, –96, and –135 mA cm^{-2}, respectively. Thus, the MnO*x* pseudocapacitance remains accessible even under current loads that cannot otherwise be sustained by O_2 reduction. For example, the highest steady-state O_2-reduction current density for the 40 wt.% MnO*x*–carbon nanofoam is –45 mA cm^{-2} (Figure 2a), while the O_2-independent pseudocapacitance supports a current density of –135 mA cm^{-2} for ~10 s to the same limiting potential (E = 0.9 V *vs.* Zn QRE, Figure 2d).

The MnO*x* pseudocapacitive contribution is finite and quickly becomes exhausted at high current/power loads as available Mn(IV) is reduced to Mn(III), as demonstrated with repeated galvanostatic discharge steps at –96 mA cm^{-2} under flowing argon, **Figure 3**a. The initial discharge pulse shows the expected linear discharge of the MnO*x* capacitance over 20 s for the 40 wt.% MnO*x*–carbon nanofoam paper. When allowed to rest at open-circuit conditions for 10 min following the initial discharge, still under argon atmosphere, the electrode potential remains below 1.2 V (Figure 3b), indicating that MnO*x* remains in its discharged, mixed-valent Mn(IV/III) state; a following discharge pulse quickly depolarizes the cell such that the potential falls from 1.2 V to the 0.9 V limit, with little capacitance provided in this or subsequent discharge pulses (Figure 3a).

Post-pulse, but in the presence of oxygen (from static air) and under open-circuit conditions, the electrode potential rapidly increases to >+1.35 V vs. Zn (Figure 3b), nearing the initial open-circuit potential recorded prior to any discharge steps. On the second and third discharge pulses, the MnO*x* pseudocapacitance that had been tapped to power the initial pulse is almost completely recovered (Figure 3c). The open-circuit recovery and renewal of capacitance indicates that after electrochemical discharge of the pseudocapacitance, Mn(III) sites spontaneously

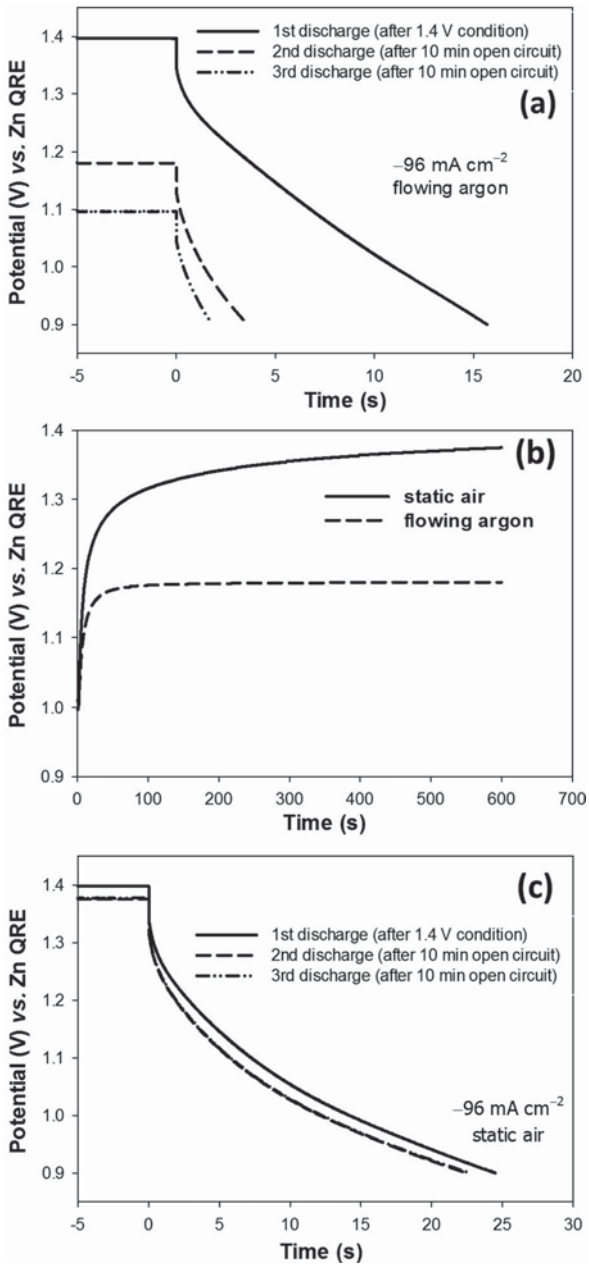

Figure 3. Galvanostatic discharge in 6 M KOH/PAA of a 40 wt.% MnO*x*-modified nanofoam paper at –96 mA cm^{-2} after 1.4-V conditioning for 20 min (—); 10-min open-circuit recovery following first discharge (– –); and 10-min open-circuit recovery following second discharge (–••–) for: (a) flowing argon atmosphere and (c) static air. The graph in (b) shows open-circuit recovery following a –96 mA cm^{-2} discharge in flowing argon (——) and static air (—).

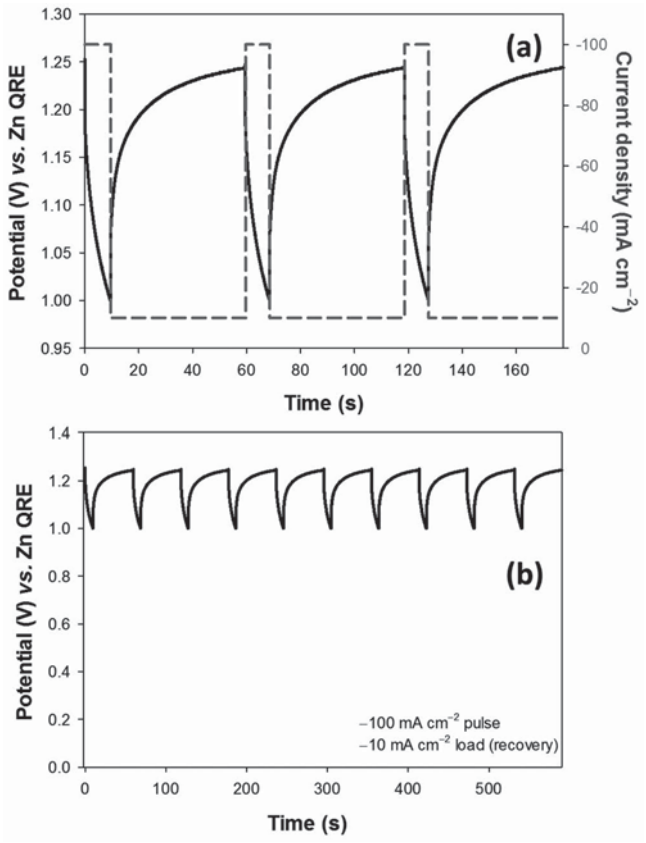

Figure 4. The potential response (—) of a 40 wt.% MnO*x*-modified carbon nanofoam paper subjected to a duty cycle (– –) consisting of periodic high-current pulses (–100 mA cm^{-2}) superimposed on a low-current baseline (–10 mA cm^{-2}), with a potential limit of 1 V vs. Zn. The scale of the y axis (b) is expanded to include 0 V *vs.* Zn QRE in order to mimic how cell potential might fluctuate in an actual Zn–air cell configuration.

re-oxidize in the presence of O_2, such that Mn(IV) sites are restored and available for reduction on subsequent discharge steps.

Oxygen-promoted regeneration of Mn(IV) has been previously reported in the context of gas-rechargeable batteries using powder-composite cathodes of 10-μm electrolytic MnO_2 powder and carbon black.[28] The recovery/recharge time for conversion of Mn(III) to Mn(IV) in electrochemically discharged MnO_2 was on the order of tens of minutes to hours, whereas with MnO*x*–carbon nanofoams, the recovery time is <100 s. The rapid recycling of the oxidation state of MnO*x* in the nanofoam-based electrode architecture is due to efficient O_2 transport through the well-plumbed pore structure and to the nanoscale morphology of the oxide coating, which obviates transport limitations that would otherwise arise from slow solid-state electron/ion diffusion within the MnO*x* domains.

With readily accessible and spontaneously rechargeable MnO*x* pseudocapacitance built into the structure of an already effective air cathode, we then explored power performance using duty cycles that alternate between providing intermittent pulse power and long-term operational load. The MnO*x*–carbon nanofoam air cathode was challenged with duty cycles that might mimic those of a functioning battery such as a Zn–air cell, by applying a low current-load baseline (–10 mA cm^{-2}) onto which we superimposed high-current cathodic pulses (–100 mA cm^{-2}) with 50-s intervals between pulses. The MnO*x* capacitance (~4.7 F cm^{-2}, delivered between ~1.18 and 1.0 V vs. Zn) sustains the demanding load for ~10 s during the high-current pulse (**Figure 4**a). We also note that the

area-normalized capacitance provided under these air-exposed, duty-cycle circumstances is comparable to that measured for single-discharge pulses under nominally O_2-free conditions (flowing argon).

During multiple repetitions of the high/low-load duty cycle, Mn(III) sites spontaneously re-oxidize even though part of the available molecular oxygen is consumed to support the applied low load via direct reduction. The degree of Mn(IV) recovery under low load is dictated by the potential assumed by the electrode, which in turn is based on the magnitude of the current demand; under a –10 mA cm^{-2} load, the electrode potential recovers to ~1.25 V, rather than 1.35 V as at the end of open-circuit recovery. The rapid, spontaneous re-oxidation of MnO*x* facilitates multiple subsequent high-load pulses, as long as sufficient low-load recovery time (~50 s) is available between pulses (Figure 4b). For a ten-pulse sequence, the power draw at –100 mA cm^{-2} was sustained for 9 s to 1 V vs. Zn for each of the ten cycles.

Our redesign of energy-storage electrodes is a marked departure from custom—we adopt an architectural approach in which the solid and void components in the macroscale electrode structure are controlled and modified on the nanoscale and remain interpenetrating over all length scales. As an air cathode, these multifunctional electrode architectures provide balanced pathways for electronic and ionic conductivity, facile permeation/transport of electrolyte and gas-phase O_2 through the 3-D interconnected void volume of the nanofoam, and maximize electrocatalytic turnover for O_2. As one would hope when bringing nanometric active components into the redesign of an established battery component, not only is performance improved (e.g., rate of oxygen influx through the porous electrode), but new function arises—pulse power is derived from the pseudocapacitance of nanoscale MnO*x*, even while the oxide fulfils its primary function of catalysing oxygen reduction in the architectured cathode. This redesign of the air cathode permits sustained periodic bursts of pulse power that are not limited by O_2 flux to the cathode and ensures rapid, spontaneous regeneration of the Mn(IV) that stores the pulse-accessible energy. By introducing an air cathode with dual function to a Zn–air cell, pulse-power capability that is otherwise missing in an energy dense and operationally safe battery, is now available. The enhanced functionality should prove beneficial for both consumer and military applications.

Supporting Information

Supporting Information is available from the Wiley Online Library or from the author.

Acknowledgements

Financial support for this work is provided by the U.S. Office of Naval Research. The authors thank Dr. Megan B. Sassin (U.S. Naval Research Laboratory) for creating the schematic shown in Figure 1.

Received: November 7, 2012
Revised: December 7, 2012
Published online: January 28, 2013

[1] D. R. Rolison, L. F. Nazar, *MRS Bull.* **2011**, *36*, 486.
[2] D. Linden, Ed., *Handbook of Batteries: Second Edition*, McGraw Hill, New York, NY **1995**.
[3] B. E. Conway, *Electrochemical Supercapacitors: Scientific Fundamentals and Techological Applications*, Plenum, New York, NY **1999**.
[4] A. Burke, *J. Power Sources* **2000**, *91*, 37.
[5] M. Conte, *Fuel Cells* **2010**, *10*, 806.
[6] A. Kuperman, I. Aharon, *Renewable Sustainable Energy Rev* **2011**, *15*, 981.
[7] D. Cericola, R. Kotz, *Electrochim. Acta* **2012**, *72*, 1.
[8] D. R. Rolison, B. Dunn, *J. Mater. Chem.* **2001**, *11* 963.
[9] J. W. Long, D. R. Rolison, *Acc. Chem. Res.* **2007**, *40*, 854.
[10] P. Sapkota, H. Kim, *J. Ind. Eng. Chem.* **2009**, *15*, 445.
[11] J. S. Lee, S. T. Kim, R. Cao, N. S. Choi, M. Liu, K. T. Lee, J. Choi, *Adv. Energy Mater.* **2011**, *1*, 34.
[12] I. Roche, E. Chainet, M. Chatenet, J. Vondrak, *J. Phys. Chem. C* **2007**, *111*, 1434.
[13] F. H. B. Lima, M. L. Calegaro, E. A. Ticianelli, *Electrochim. Acta* **2007**, *52*, 3732.
[14] D. R. Rolison, J. W. Long, J. C. Lytle, A. E. Fischer, C. P. Rhodes, M. E. Bourg, A. M. Lubers, *Chem. Soc. Rev.* **2009**, *38*, 226.
[15] J. C. Lytle, J. M. Wallace, M. B. Sassin, A. J. Barrow, J. W. Long, J. L. Dysart, C. H. Renninger, M. P. Saunders, N. L. Brandell, D. R. Rolison, *Energy Environ. Sci.* **2011**, *4*, 1913.
[16] A. E. Fischer, K. A. Pettigrew, D. R. Rolison, R. M. Stroud, J. W. Long, *Nano Lett.* **2007**, *7*, 281.
[17] A. E. Fischer, M. P. Saunders, K. A. Pettigrew, D. R. Rolison, J. W. Long, *J. Electrochem. Soc.* **2008**, *155*, A246–A252.
[18] M. B. Sassin, C. N. Chervin, D. R. Rolison, J. W. Long, *Acc. Chem. Res.* **2013**, DOI: 10.1021/ar2002717
[19] J. W. Long, M. B. Sassin, A. E. Fischer, D. R. Rolison, A. N. Mansour, V. S. Johnson, P. E. Stallworth, S. G. Greenbaum, *J. Phys. Chem. C* **2009**, *113*, 17595.
[20] M. B. Sassin, C. P. Hoag, B. T. Willis, N. W. Kucko, D. R. Rolison, J. W. Long, *Nanoscale*, **2013**, DOI: 10.1039/c2nr34044e
[21] C. N. Chervin, J. W. Long, N. L. Brandell, J. M. Wallace, N. W. Kucko, D. R. Rolison, *J. Power Sources* **2012**, *207*, 191.
[22] I. Roche, E. Chainet, M. Chatenet, J. Vondrak, *J. Phys. Chem. C* **2007**, *111*, 1434.
[23] L. Q. Mao, D. Zhang, T. Sotomura, K. Nakatsu, N. Koshiba, T. Ohsaka, *Electrochim. Acta* **2003**, *48*, 1015.
[24] W. Xiao, D. Wang, X. W. Lou, *J. Phys. Chem. C* **2010**, *114*, 1694.
[25] H. Y. Lee, J. B. Goodenough, *J. Solid State Chem.* **1999**, *144*, 220.
[26] M. Toupin, T. Brousse, D. Bélanger, *Chem. Mater.* **2004**, *16*, 3184.
[27] P. Guillemet, T. Brousse, O. Crosnier, Y. Dandeville, L. Athouel, Y. Scudeller, *Electrochim. Acta* **2012**, *67*, 41.
[28] B. Choi, S. Lee, C. Fushimi, A. Tsutsumi, *Electrochim. Acta* **2010**, *55*, 8771.